RSC Advances

PAPER

View Article Online
View Journal | View Issue



Cite this: *RSC Adv.*, 2025, **15**, 29160

# Synthesis of novel N1 functionalized diazepinone analogues *via* a base-mediated C–N cross coupling reaction as reverse transcriptase inhibitors: theoretical and experimental investigations

Shivangi Jaiswal,[a] Smita Jain,[b] Achal Mukhija,[a] Kanika Verma,[c] Sonika Jain,[a] Dharma Kishore,[a] Jaya Dwivedi *[a] and Swapnil Sharma[d]

The sodium hydrogen orthophosphate ($Na_2HPO_4$) base was utilized in a stereospecific C–N coupling reaction to synthesize a novel series of nevirapine analogues in two-step reactions. This base is moisture tolerant, commercially available and makes the protocol cheap and energy efficient, with broad substrate tolerance, leading to the formation of cyclopropyl, cyclobutyl, cyclopentyl and propane-engrafted dipyridodiazepinone derivatives in good yield with a higher atom economy >70%. All the synthesized analogues were examined for reverse transcriptase inhibitory activity and compared with the reference drug nevirapine. Further *in silico* analysis *via* molecular docking, molecular simulation, and ADMET studies revealed that compounds **5a** and **5b** showed prominent inhibitory activity against reverse transcriptase. Additionally, isothermal titration calorimetry experiments were performed to determine the thermodynamic parameters of the interaction between nevirapine analogues and human serum albumin. The binding affinity of **5b** in the order of $10^2$ indicates that the synthesized analogues can be easily carried out into the bloodstream. These findings demonstrate that nevirapine analogous are promising reverse transcriptase inhibitors for the therapeutic treatment of HIV infection, offering a new avenue for the less toxic and more effective development of anti-retroviral drugs.

Received 18th May 2025
Accepted 30th July 2025

DOI: 10.1039/d5ra03504j

rsc.li/rsc-advances



## 1 Introduction

Seven-membered nitrogen-containing diazepine framework is a core heterocyclic skeleton in various bioactive agents, including compounds with antidepressant, antibacterial, antiviral, antifungal and antitumor activities.[1–4] Many reports have revealed that benzodiazepine and pyridodiazepine in zapizolam, clozapine and olanzapine possess good anti-anxiety, anticonvulsant, sleep-inducing and muscle relaxant properties, while the dipyridodiazepinone skeleton in nevirapine plays a pivotal role in inhibiting the reverse transcriptase enzyme (Fig. 1).[5,6] This enzyme is responsible for converting RNA into DNA and promoting the replication of retroviruses in host cells.[7] Most importantly, diazepine motifs have received increasing interest in clinical practice and drug discovery. Hence, new strategies for constructing dipyridodiazepinone scaffolds have received considerable attention, and this skeleton is suitable for the design and development of more effective compounds for the treatment of HIV infections and related issues.

In recent years, the C–N coupling reaction has been very powerful for the construction of complex molecules from simple synthons.[8–10] Among coupling reactions, the Buchwald–Hartwig cross coupling reaction has attracted great attention for intermolecular and intramolecular coupling, resulting in the formation of a cyclic ring, *i.e.* a seven-membered diazepine ring. Previously, this reaction was assisted by caesium carbonate and a metal catalyst, mainly palladium catalysts, with additional ancillary ligands. Currently, metal-free and highly atom-economical methods are being explored worldwide for the synthesis of nitrogen heterocycles *via* coupling reactions.

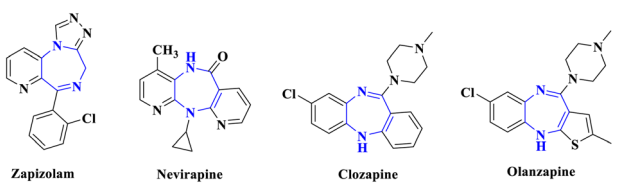


Fig. 1 Representative bioactive diazepine derivatives.

[a]*Department of Chemistry, Banasthali Vidyapith, Banasthali, Rajasthan, India. E-mail: jayadwivedi@yahoo.co.in*

[b]*Department of Pharmacy, School of Chemical Sciences and Pharmacy, Central University of Rajasthan, Kishangarh, Rajasthan, India*

[c]*Department of Internal Medicine, Division of Cardiology, LSU Health Sciences Center–Shreveport, Louisiana, USA*

[d]*Department of Pharmacy, Banasthali Vidyapith, Banasthali, Rajasthan, India*

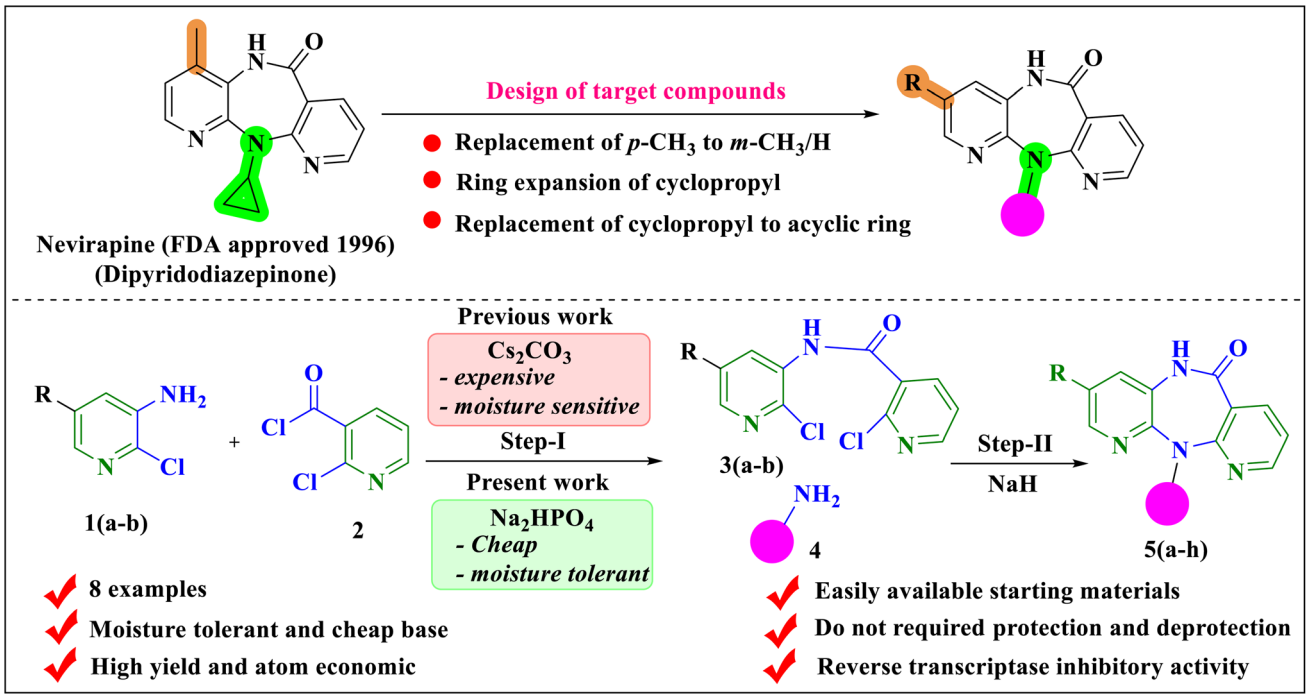


Fig. 2 Preparation of designed compounds in a two-step synthetic process *via* C–N coupling.

The principal objective of the present study is the cost-effective synthesis of novel dipyridodiazepinones, which are analogues of nevirapine. The present study reports the design of dipyridodiazepinone analogues using pharmacophore modelling and synthesizes them *via* base-promoted C–N coupling and cyclocondensation reactions (Fig. 2).

The synthesized analogues were examined for an inhibitory effect against the HIV-1 RT enzyme. Furthermore, a spectrum of computational studies including MD simulation, ADMET/pharmacokinetics analysis, physicochemical analysis, *in silico* drug likeness, and molecular docking were performed. Additionally, the thermodynamic parameter of the binding interaction of synthesized compounds with human serum albumin (HSA) was investigated using isothermal titration calorimetry experiments. It is imperative to achieve the thermodynamic and binding parameters of the synthesized analogues to the macromolecules. Understanding thermodynamics and binding parameters is crucial for physicochemical mechanisms, such as the pharmacokinetics and pharmacodynamics of the synthesized dipyridodiazepinone.[11] Serum albumins are the most abundant protein in blood plasma responsible for the transportation of drugs in the circulatory system. The physiological role of the serum protein is to transport numerous ligands, such as amino acids, fatty acids, steroids, drugs, and metal ions, in the bloodstream to the targeted organs. In the circulatory system, serum albumin plays a major role in binding synthesized compounds or drugs and further transporting them to the target site. Thus, the binding of synthesized compounds to serum albumin is a pharmacokinetic criterion. The availability of the free drug is inversely proportional to the binding constant of serum albumin to the ligand. It means that when the binding is stronger, the availability of free drug is lower in the blood. Similarly, if the binding is weaker, the amount of free drug in the circulation is greater.[12] To understand the pharmacokinetic and ADMET mechanisms, knowledge of the binding interaction between the drug and protein is important. From this perspective, particular attention has been given to HSA, the most important plasma protein and the main carrier for transporting metabolites and drugs into the bloodstream.

## 2 Results and discussion

### 2.1 Feature mapping analysis using a structure-based pharmacophore

The computer-aided drug design process, such as structure-based pharmacophore modeling, is useful for identifying possible lead compounds that inhibit the HIV reverse transcriptase enzyme. Discovery Studio 2.0 is used to develop a six-feature pharmacophore model consisting of two hydrogen bond acceptors (HBA), two hydrophobic features (HY), and two hydrogen bond donors (HBD), as shown in Fig. 3. Feature mapping of the synthesized compounds **5(a–h)** on the developed HIV RT enzyme's structure-based pharmacophore and observed that **5a** and **5b** showed four feature mappings with 2.42008 and 2.59238 fit values. The PharmPrint of the synthesized analogues is shown in SI Table S1.

### 2.2 Chemistry

The exploration of the concept of the C–N coupling reaction in the synthesis of new nevirapine analogues is formulated in Scheme 1. The synthesis of carboxamide **3(a–b)** was achieved by the intermolecular C–N coupling reaction of **1(a–b)** with 2-

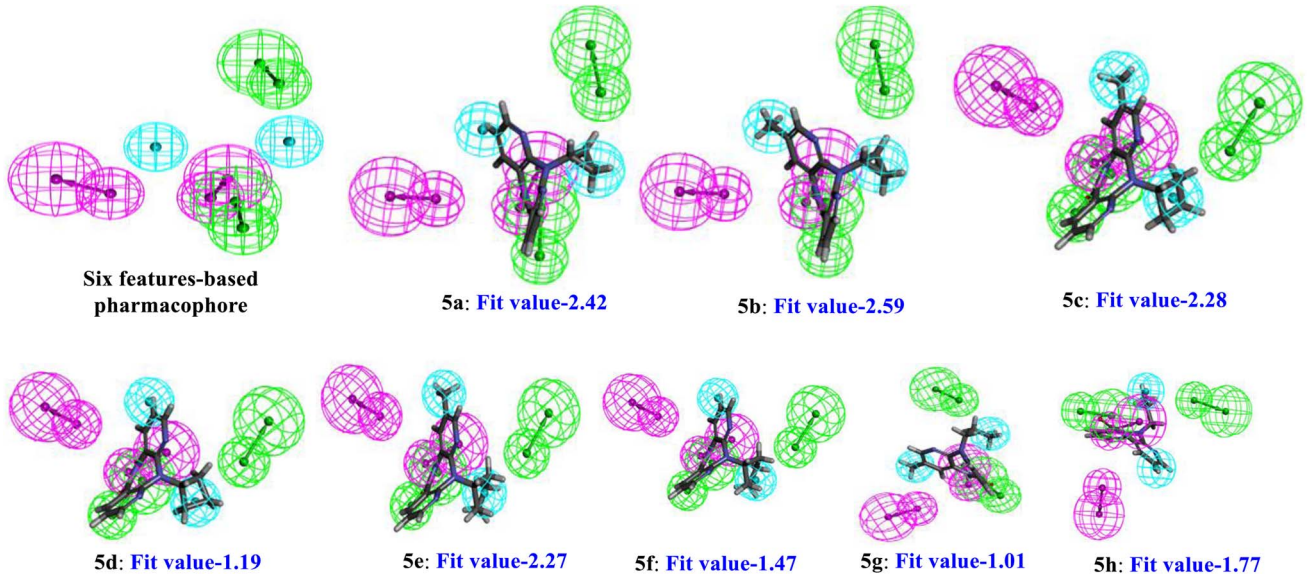


Fig. 3 Feature mapping analysis of 5(a–h) using structure-based pharmacophore modelling (green colour: HBA, cyan colour: HY, and pink colour: HBD).

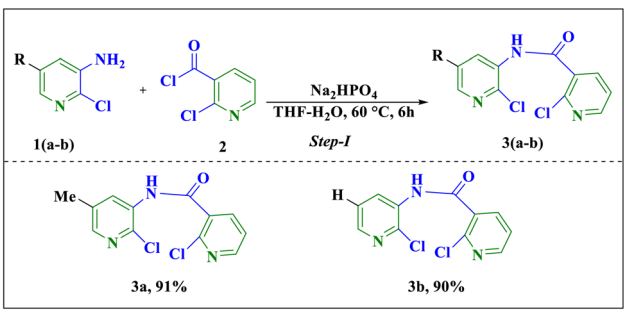


Scheme 1 Synthesis of carboxamide 3(a–b).

chloronicotinyol chloride **2** in the presence of base sodium hydrogen orthophosphate ($Na_2HPO_4$). The formation of compounds **3(a–b)** was established by their $^1$H NMR spectra, which showed a sharp singlet at $\delta$ 8.8 ppm for one proton attached to nitrogen.

Compound **3(a–b)** underwent an intermolecular coupling on its treatment with cyclopropylamine, cyclobutylamine, cyclopentylamine and propylamine in $Na_2HPO_4$; then, intramolecular coupling resulted in cyclization to form 1,4-dipyridiodiazepinone **5(a–h)** (Scheme 2). The $^1$H-NMR, $^{13}$C-NMR, and mass spectral analysis were used to confirm the structures and purity of the synthesized nevirapine analogues. The result of the HSQC NMR experiment confirms the assignment of the NH signal at 8.87 ppm, as it shows no direct correlation to any carbon signal, consistent with the presence of a non-carbon-bound proton. This observation validates the presence of an NH group in the structure of compound **3a**. Compared to starting material 2-chloro-3-aminopyridine **1(a–b)**, the most relevant variation in the NMR spectra arises owing to the amide and amine coupling. The spectra of nevirapine analogues were in accordance with the structure of synthesized analogues shown in SI S1–S42.

Initially, 3-amino-2-chloro-5-methyl pyridine **1a** and 2-chloronicotinyol chloride **2** were selected as the model substrates to optimize the reaction conditions (Table 1). This reaction was carried out in potassium carbonate $K_2CO_3$ and 1,4-dioxane at 60 °C for 6 h, and only a 20% yield was obtained. The change in solvent from 1,4-dioxane to THF results in an increase in yield from 20% to 40% (entry 2). Next, the caesium carbonate base is tested with solvent 1,4-dioxane; again, a decrease in the yield of the product was observed (entry 3). The same base tested with solvent THF showed an increase in yield (entry 4). We hypothesized that a change in the solvent system would affect the yield of the reaction owing to the solubility of the starting reactant and ion pairing. Further, to increase the yield from 50%, the solvent effect was further explored using a mixture of THF–$H_2O$ (entry 5). Encouraged by the result, $Na_2HPO_4$ base utilized in THF–$H_2O$ (5 : 2) solvent showed the best conversion with a maximum yield of 91% (entry 6). In further exploration, an increase in the ratio of water provided 80% and 75% yields of **3a** (entry 7–8). Finally, a reaction was performed on triethylamine, and a trace yield of the product was achieved (entry 9). The amide bond difference in products **3a** and **3a′** was confirmed by FTIR spectroscopy, as evidenced by distinct variations in the carbonyl stretching frequencies of 1650 cm$^{-1}$ and 1725.04 cm$^{-1}$, respectively, as shown in SI S2 and S3. The spot of the TLC plate indicates a favorable C–N coupling reaction between the amine of compound **1a** and the carbonyl chloride of compound **2** in base $Na_2HPO_4$ to form **3a** in good yield.

Under the best optimized conditions (Table 1, entry 6), the substrate scope of various cyclic and acyclic amines, such as cyclopropyl amine, cyclobutyl amine, cyclopentyl amine and propyl amine, was investigated in C–N coupling reaction and

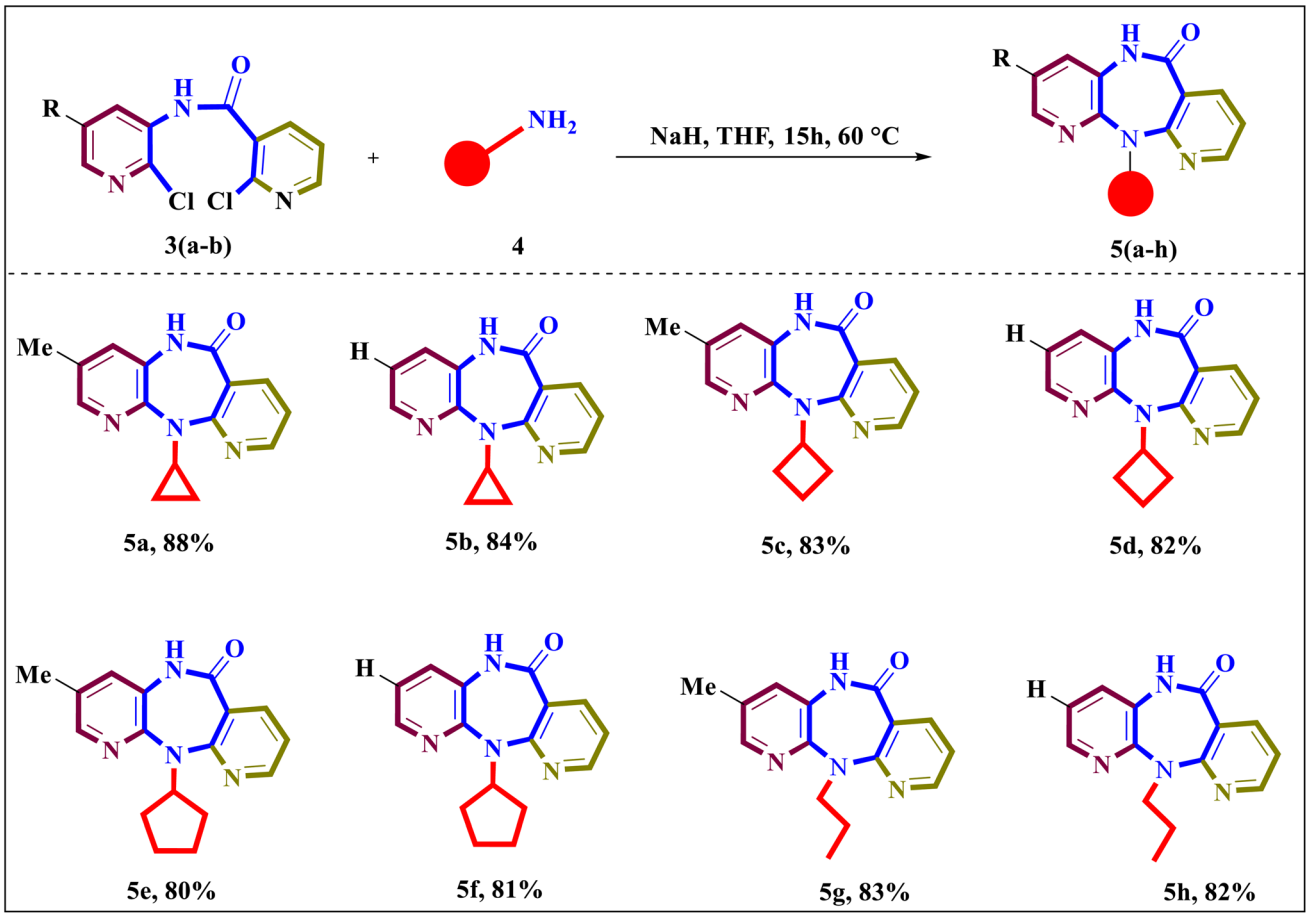


Scheme 2 Substrate scope for the synthesis of novel dipyridodiazepinone derivatives.

Table 1 Optimization of reaction conditions[a]

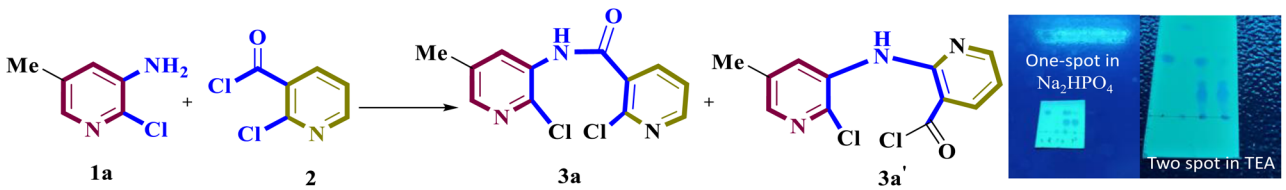


| S. no. | Base | Solvent | Temp./time | Yield (3a) | Yield (3a′) |
|---|---|---|---|---|---|
| 1 | $K_2CO_3$ | 1,4-Dioxane | 60 °C, 6 h | 20% | — |
| 2 | $K_2CO_3$ | THF | 60 °C, 6 h | 40% | — |
| 3 | $Cs_2CO_3$ | 1,4-Dioxane | 60 °C, 6 h | 24% | — |
| 4 | $Cs_2CO_3$ | THF | 60 °C, 6 h | 50% | — |
| 5 | $Cs_2CO_3$ | THF–$H_2O$ (5 : 2) | 60 °C, 6 h | 60% | — |
| 6 | $Na_2HPO_4$ | THF | 60 °C, 6 h | 82% | — |
| 7 | $Na_2HPO_4$ | THF–$H_2O$ (5 : 2) | 60 °C, 6 h | 91% | 1% |
| 8 | $Na_2HPO_4$ | THF–$H_2O$ (4 : 3) | 60 °C, 6 h | 80% | 2% |
| 9 | $Na_2HPO_4$ | THF–$H_2O$ (3 : 4) | 60 °C, 6 h | 75% | Trace |
| 10 | TEA | THF | 60 °C, 6 h | Trace | Trace |

[a] Reaction conditions: **1a** (0.0187 mmol), 2 (0.0187 mmol), $Na_2HPO_4$ (0.02 mmol), 6 h, and temperature 60 °C in sealed tube.

cyclization (Scheme 2). It is noteworthy that the size of the ring influences the yield of the product. The smaller cyclopropylamine has a higher yield than cyclopentyl amine due to exhibiting steric hindrance in C–N cross coupling reactions. A good to high yield was obtained, where R is substituted with a methyl or hydrogen group. Noteworthy, **5a** and **5b** were obtained in higher yields, followed by substituents with cyclobutyl amine (**5c–5d**), cyclopentyl amine (**5e–5f**) and propyl amine (**5g–5h**). The larger substituents might cause steric hindrances, which further prevent intermolecular cyclocondensation from forming the diazepine ring.

Further series of control experiments were conducted to gain insight into this reaction, as outlined in Scheme 1. The initial radical inhibition experiment was performed using TEMPO. The result showed that a product yield 77% was obtained and the reaction was not inhibited, which clearly stated that the radical mechanism was not involved (Scheme 3a). According to previous reports, we hypothesized that the reaction involves amidation, amination and cyclocondensation reaction.[13] For further investigation, we synthesized intermediates **3A** and **3B** at 60 °C, giving 85% and 91% yields in Scheme 3b and c, respectively. Both intermediates under standard conditions produced **5a** in 50% and 88%, respectively. These outcomes suggest that the formed intermediate might be responsible for accelerating the reaction. The mechanism is proposed based on the control experiment results, as outlined in SI Scheme S1. Further sustainability of the reaction pathway was examined by evaluating the atom economy. The synthesized compounds have an atom economy greater than 70%, indicating that the process is sustainable with minimum waste generation. The atom economy of the synthesized compounds is in the following order: **5a** (71%), **5b** (70%), **5c** (72%), **5d** (71%), **5e** (73%), **5f** (72%), **5g** (71%), and **5h** (70%).

### 2.3 HIV-1 reverse transcriptase inhibitory activity

The synthesized dipyridodiazepinone analogue **5(a–h)** was screened *in vitro* for reverse transcriptase inhibitory effect using the HIV-1 RT ELISA kit. Among all, analogue **5b** ($IC_{50} = 0.86$ nM) was the most potent, followed by **5a** ($IC_{50} = 1.07$ nM), when compared with standard nevirapine ($IC_{50} = 3.05$ nM). The results of the HIV-1 RT assay for all synthesized analogues are

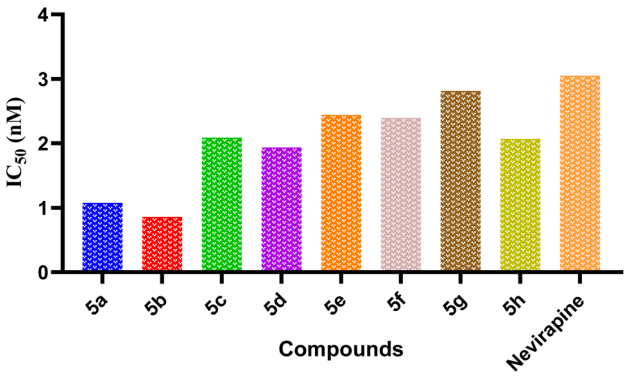


Fig. 4 Inhibitory effect of synthesized analogues on the HIV-RT enzyme.

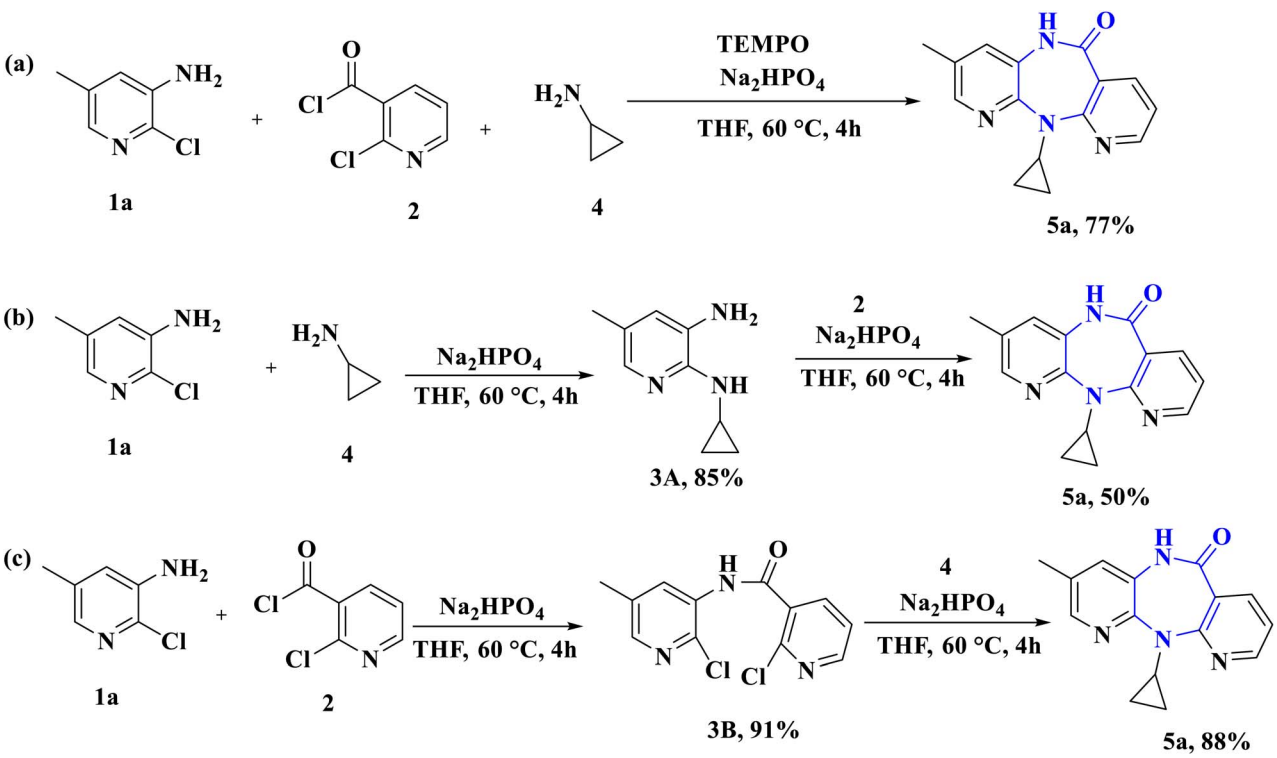


Scheme 3 (a–c) Control experiments.

shown in Fig. 4. The activity data indicate that cyclopropyl substituents in **5a** and **5b** showed prominent inhibitory activity compared to cyclobutyl, cyclopentyl and alkyl substituted dipyridodiazepinone derivatives.

### 2.4 Molecular docking

A molecular docking study is a crucial tool for evaluating the interaction between the target protein and drug. In this current *in silico* study, dipyridodiazepinone analogues (**5a**, **5b**, **5c**, **5d**, **5e**, **5f**, **5g** and **5h**) were docked against HIV-1 reverse transcriptase using the Auto-Dock Vina module. The docking scores of all synthesized compounds are shown in Table 2. The binding site of the HIV-1 reverse transcriptase is surrounded by the 10 amino acid residues *viz.* Lys101, Lys103, Val179, Val106, Leu100, Tyr318, Tyr188, Tyr181, Pro95 and Trp229. We found that among all synthesized compounds, nevirapine analogues **5a** and **5b** had higher binding energies of −9.5 kcal mol$^{-1}$ and −9.8 kcal mol$^{-1}$ when compared to nevirapine −9.2 kcal mol$^{-1}$, as shown in Table 2. This prompted the initiative to visualize their binding pose and interaction patterns with the target proteins relative to the reference drug (nevirapine) using PyMol and Discovery Studio Visualizer. The analogues were observed to fit into the same cavity of the binding sites. Interestingly, in **5a**, the amino group of the diazepin-6-one ring was involved in the one hydrogen bond formation within the binding cavities of macromolecules, such as Lys101 at a bond length of 2.10 Å. A pi–sigma bond with 3.82 Å was observed between the diazepin-6-one ring and Leu100 amino acid residues, while **5a** compound was also involved in the formation of alkyl and pi–alkyl bond interactions with the Val106 (3.89, 4.68 Å), Leu234 (4.65 Å), Tyr188 (4.66 Å), Tyr181 (5.27 Å), Val179 (4.23 Å), and Lys103 (5.20 Å) amino acid residues of the macromolecules. In the **5b** compound, the diazepin-6-one ring was involved in hydrogen bond formation with Lys101 amino acid residues at a 2.05 Å bond length. Similarly, the diazepin-6-one ring was involved in the formation of a pi–sigma bond with the Leu100 (4.54 Å) amino acid residue of the macromolecule, while the **5b** compound was also involved in the formation of alkyl and pi–alkyl bond interactions with the Lys103 (5.29 Å), Tyr181 (4.83 Å), Val106 (3.86, 4.90 Å), Leu234 (4.51 Å), and Tyr188 (4.83 Å). The reference drug, nevirapine, used in this study showed a comparable binding energy of −9.2 kcal mol$^{-1}$. The amide group of the diazepinone ring was able to form one hydrogen bond with Lys 101 at a distance of 2.54 Å. Meanwhile, Leu 103 established a carbon–hydrogen bond at a distance of 4.60 Å. Tyr188 (4.51 Å), Val 106 (5.49, 4.36 A), Tyr 318 (4.59 A), Tyr 188 (4.51 A), Tyr 181 (5.24 A), Val 179 (5.04 A), and Leu 100 (4.60, 3.93, 3.74 A) were associated with the reference drug *via* alkyl and pi–alkyl bonds, as shown in Fig. 5. The binding interactions of **5c**, **5d**, **5e**, **5f**, **5g** and **5h** are shown in SI (Fig. S1–S6). The results from molecular docking suggest that amino acids, such as leucine, valine, and tyrosine, are vital for binding ligands to the HIV-1 RT active site. In conclusion, the docking results were in line with the *in vitro* assay and indicated that the synthesized analogues might be potential inhibitors of HIV-1 RT.

### 2.5 ADMET

The findings of the drug-likeness and physicochemical studies provide supporting evidence for the drug-like properties of the synthesized analogues (Table 3). According to the results, nevirapine and its analogues **5a**, **5b** had log $P$ ($C$ log $P$) < 5, molecular weight < 500, fewer than 10*H*-bond acceptors, and 5*H*-bond donors. These findings indicate that the synthesized analogues follows Lipinski's rule of 5 and exhibit drug-like properties.

ADMET analysis was conducted to define the pharmacological profile of nevirapine and its synthesized analogues, which paves the way for predicting it as a drug candidate. Drug

Table 2 Binding energies of synthesized analogues docked against the HIV-I reverse transcriptase enzyme[a]

| Compounds | Binding energy (kcal mol$^{-1}$) | Amino acid residues with distance (Å) |
|---|---|---|
| **5a** | −9.5 | H-Lys101 (2.10), C-Lys103 (5.20), C-Val106 (3.89, 4.68), C-Tyr188 (4.66), C-Tyr181 (5.27), C-Val179 (4.23), C-Leu100 (3.82) |
| **5b** | −9.8 | H-Lys101 (2.18), C-Leu100 (3.57), C-Lys103 (5.29), C-Leu234 (4.58), C-Tyr181 (4.83), C-Tyr188 (4.83), C-Val106 (3.86, 4.90) |
| **5c** | −8.3 | H-Lys101 (1.98), C-Leu234 (4.82), C-Tyr318 (5.47), C-Tyr188 (4.38), C-Tyr181 (5.40), C-Val106 (3.84, 4.54) |
| **5d** | −8.4 | H-Lys101 (1.97), C-Leu234 (4.75), C-Tyr318 (5.45), C-Val106 (3.87, 4.56), C-Tyr188 (4.45), C-Tyr181 (5.38), C-Lys103 (5.22, 5.17), C-Lys101 (4.55), C-Val179 (4.61) |
| **5e** | −8.5 | H-Lys101 (2.55), C-Tyr188 (3.75, 4.63), C-Val106 (4.22), C-Lys103 (5.13), C-Tyr318 (4.89), C-Trp229 (3.87, 3.63), C-Tyr318 (4.89) |
| **5f** | −8.9 | H-Lys101 (2.13), O-Lys101 (3.21), C-Val106 (4.10), C-Lys103 (5.26), C-Tyr188 (4.34), C-Tyr181 (5.31), C-Trp229 (4.87, 4.89), C-Leu100 (4.87, 3.57, 3.81, 4.82) |
| **5g** | −8.7 | H-Lys101 (2.05), C-Tyr188 (3.90), C-Tyr181 (4.91), C-Leu100 (4.28), C-Leu100 (3.74, 4.31), C-Lys101 (4.26), C-Val179 (4.28), C-leu234 (4.55), C-Val106 (3.89) |
| **5h** | −9.0 | H-Lys101 (2.07), C-Tyr181 (4.87), C-Tyr188 (3.84), C-Leu100 (4.32), C-Leu100 (3.72, 4.24), C-Val106 (3.85, 4.81), C-Leu234 (4.59) |
| NVP | −9.2 | H-Lys101 (2.18), C-Leu100 (3.57), C-Tyr188 (4.53), C-Leu234 (4.58), C-Phe227 (5.28), C-Lys103 (4.45), C-Tyr318 (4.40), C-Val106 (4.60) |

[a] NVP: nevirapine (standard drug).

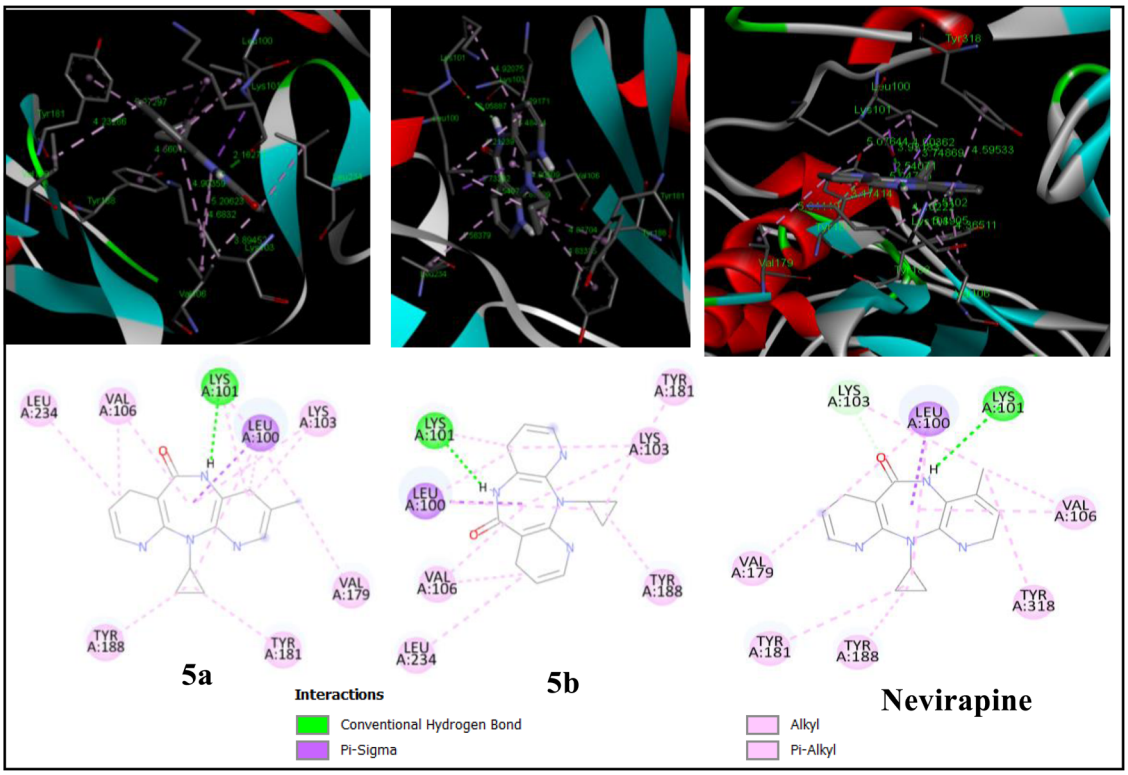


Fig. 5 Binding interactions of **5a**, **5b** and nevirapine with the active binding pockets of HIV-I reverse transcriptase enzyme.

Table 3 Drug-like, physicochemical, and ADMET properties

| Class | Properties | 5a | 5b | NVP |
|---|---|---|---|---|
| Physicochemical properties | Molecular weight (g mol$^{-1}$) | 266 | 252 | 266 |
| | Lipophilicity ($c\log P$) | 1.96 | 1.62 | 1.96 |
| | Solubility | −4.67 | −4.32 | −4.67 |
| | TPSA (Å) | 58.12 | 58.12 | 58.12 |
| | Drug likeness | 3.02 | 3.09 | 3.02 |
| | Drug score | 0.73 | 0.78 | 0.73 |
| | H bond acceptor | 4 | 4 | 4 |
| | H bond donor | 1 | 1 | 1 |
| | Rotatable bond | 1 | 1 | 1 |
| | Violation | 0 | 0 | 0 |
| | Bioavailability score | 0.55 | 0.55 | 0.55 |
| Absorption | GI absorption | High | High | High |
| Metabolism | CYP3A4 substrate | ✗ | ✗ | ✓ |
| | CYP2D6 substrate | ✗ | ✗ | ✗ |
| | CYP1A2 inhibitor | ✓ | ✓ | ✓ |
| | CYP2C9 inhibitor | ✗ | ✗ | ✗ |
| | CYP2C19 inhibitor | ✓ | ✗ | ✗ |
| | CYP3A4 inhibitor | ✗ | ✓ | ✗ |
| | CYP2D6 inhibitor | ✗ | ✗ | ✗ |
| Distribution | BBB | High | High | High |
| | Plasma protein binding (PPB) | ✓ | ✓ | ✓ |
| Excretion | Total clearance (log ml min$^{-1}$ kg$^{-1}$) | 0.005 | 0.02 | 0.02 |
| Toxicity | AMES mutagenicity | ✗ | ✗ | ✗ |
| | Oral rat acute toxicity ($LD_{50}$) (mol kg$^{-1}$) | 2.494 | 2.529 | 2.644 |
| | Hepatotoxicity | ✓ | ✓ | ✓ |
| | Skin sensitisation | ✗ | ✗ | ✗ |
| | Carcinogenicity | ✗ | ✗ | ✗ |

candidates demonstrated inadequate absorption when their topological polar surface area (TPSA) exceeds the threshold of 140 Å$^2$, which serves as a baseline for approved pharmaceuticals. There exists a positive association between TPSA and mass, wherein molecules with a mass above 500 g mol$^{-1}$ were reported to exhibit TPSA values outside the range of 0–140. The TPSA values and Gastrointestinal Absorption (GIA) of the retrieved analogues were deemed satisfactory.[14] A bioavailability score larger than zero, *i.e.* 0.55, suggests that the analogues exhibit at least 10% oral bioavailability or measurable Caco-2 permeability, contributing to their drug-like property. The permeability characteristics of a medication, namely its GIA and Blood–Brain Barrier (BBB) permeability, have significant importance in the context of developing a treatment intended for extensive use.

Many previous studies have been conducted to enhance the gastrointestinal penetration of molecules for the oral delivery of poorly absorbed medications.[15] All three compounds demonstrated satisfactory growth inhibitory activity and were able to penetrate the blood–brain barrier. Cytochrome P450s (CYPs) are an imperative group of enzymes, including heme, and play a substantial role in metabolising pharmaceutical compounds and eliminating foreign substances. CYP activity might be affected by pharmaceutical agents, resulting in noteworthy drug–drug interactions with potential clinical implications. These interactions may give rise to therapeutic inefficacy or unexpected side effects. It is noteworthy that **5a**, **5b**, and nevirapine do not inhibit enzymes CYP2C9, CYP2D6, and CYP3A4, indicating that they have increased chances of being eliminated and metabolized through the metabolic biotransformation process at a substantial rate. The acute toxicity prediction assays, including the AMES test, acute oral toxicity, skin sensitization, and hepatotoxicity, revealed **5a**, **5b**, and nevirapine to be non-toxic, non-carcinogenic, non-mutagenic, and non-irritant. Although **5a**, **5b**, and nevirapine were predicted to be hepatotoxic, these effects might be produced at a higher dose range. Notably, according to the Globally Harmonized System (300 < category 4 ≤ 2000 mg per kg per day), $LD_{50}$ values found within the range of 1266–2175 mg per kg per day were considered in category 4, indicating that **5a** and **5b** are non-toxic.[16] Consequently, based on preliminary drug-likeness, physicochemical, and ADMET prediction studies, **5a** and **5b** may be promising candidates for further investigations.

### 2.6 Molecular simulation

The synthesized analogues showed inspiring results *in silico* and drug-likeness studies; the analogues were screened for MD simulation studies.[17,18] MD simulations on the analogues were conducted using the Desmond package with significant predicted binding energies (>−70.00 kcal mol$^{-1}$). The binding energies were calculated between the HIV-I reverse transcriptase protein and synthesized analogues. The **5a** and **5b** exhibited −73.53 kcal mol$^{-1}$ and −86.44 kcal mol$^{-1}$ binding energies, respectively (Fig. 6 and 7). In the current investigation, the stability of novel synthesized nevirapine analogues (**5a** and **5b**) and enzyme (1tkx) complexes were identified using HIV-I reverse transcriptase and 100 ns MD simulations.

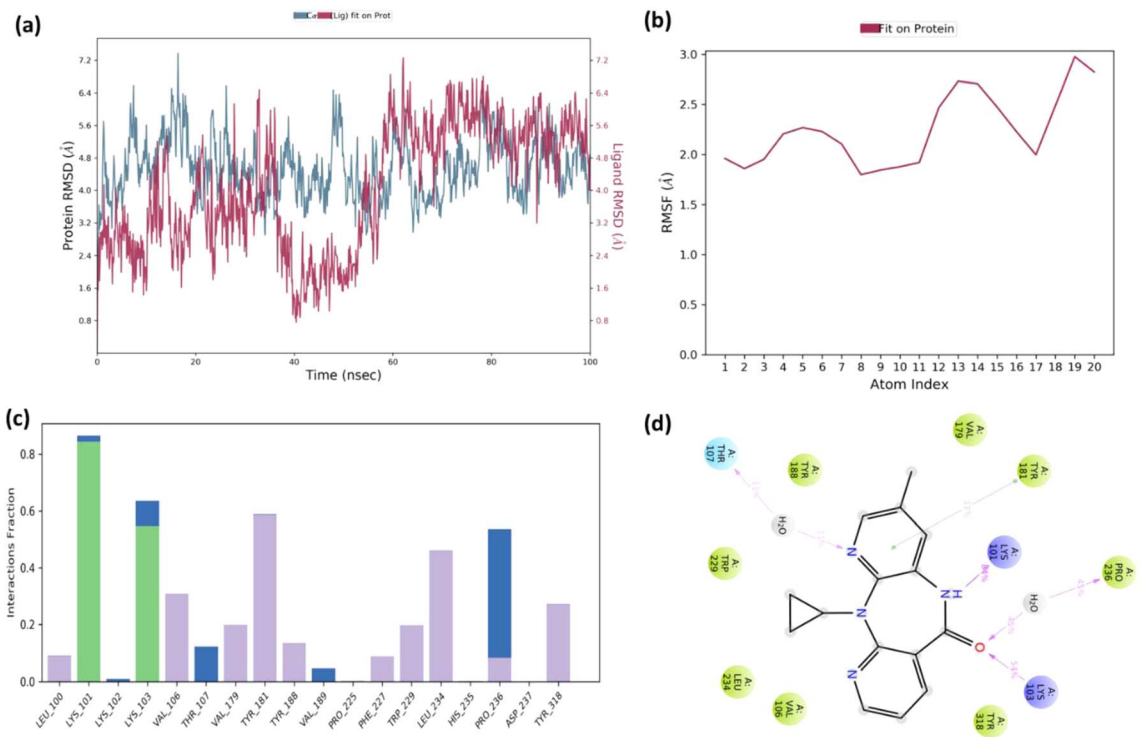


Fig. 6 (a) RMSD analysis of **5a**, (b) RMSF analysis of **5a**, (c) binding interaction analysis of **5a** with the HIV-I reverse transcriptase, and (d) 2D-contact information of **5a** with the HIV-I reverse transcriptase enzyme.

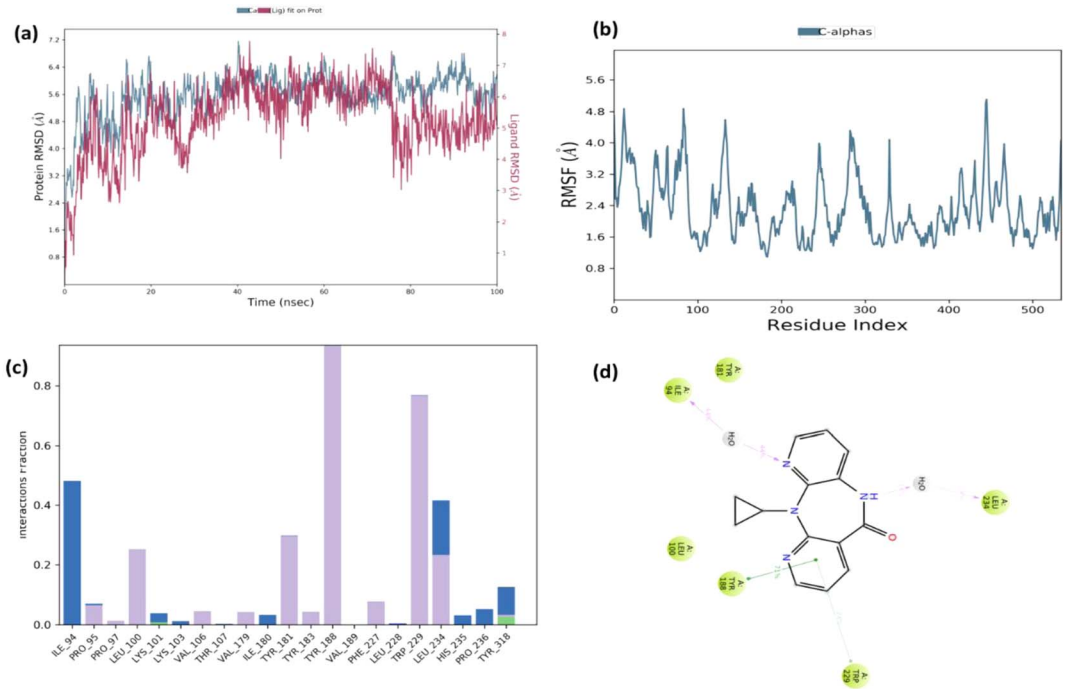


Fig. 7 (a) RMSD analysis of **5b**, (b) RMSF analysis of **5b**, (c) binding interaction analysis of **5b** with the HIV-I reverse transcriptase, and (d) 2D-contact information of **5b** with the HIV-I reverse transcriptase enzyme.

The root mean square deviation (RMSD) calculates the average distance caused by atom displacement for a given time frame. RMSD analysis can be used to establish the occurrence of equilibrated simulation. Notably, fluctuations between the range of 1–3 Å are considered perfectly acceptable within a reference protein structure. A significant conformational change in the structure of a protein indicates an unstable system. During a 100 ns simulation experiment, analogues **5a** and **5b** exhibited an extended variation of 4.53 Å and 5.57 Å, respectively, as presented in SI (Table 2). According to the results, HIV-1 reverse transcriptase undergoes a protein conformational change as a result of binding with analogues. Analogue **5a** showed minimal structural modifications within the range of 32–46 Å, suggesting a rather stable alignment throughout the binding region (SI (Fig. S7a)). Similarly, **5b** was involved in the hydrogen bond formation with Lys101 and Tyr318 amino acid residues; hydrophobic interactions with Pro95, Pro97, Tyr181, Val179, Val106, Leu100, Tyr183, Tyr188, Phe227, Trp229, and Leu234 and water bridge interactions with Ile94, Pro95, Lys101, Lys103, Ile180, His235 and Pro236 amino acid residues of HIV-I RT enzyme. Similarly, **5b** showed minimal structural modifications ranging from 28 to 38 Å, suggesting a rather stable alignment within the binding site (SI (Fig. S7c)). The molecular docking and molecular dynamics simulation results showed that compounds **5a** and **5b** exhibited hydrogen bond interaction (hydrophilic interaction) with the Lys101 amino acid residue of the HIV-1 reverse transcriptase enzyme. Similarly, both compounds **5a** and **5b** formed hydrophobic interactions with various Leu234, Val106, Lys103, Leu100, Tyr188, Tyr181 and Val179 amino acid residues of HIV-1 reverse transcriptase enzyme. These amino acid residues represent the allosteric binding sites of the HIV-1 RT enzyme.[19] The literature review demonstrates that an allosteric binding site of the HIV-1 RT enzyme, also named the NNRTIBP (non-nucleoside reverse transcriptase inhibitors binding pockets), is located within the primer grip region near the polymerase's active site, which lies primarily in the p66 region of the polymerase active site.[20,21] It comprises several aromatic (Tyr181, Tyr188, Phe227, Trp229 and Tyr232), hydrophilic (Lys101, Lys103, Ser105, Asp132, and Glu224), and hydrophobic residues (Pro59, Leu100, Val106, Val179, and Leu236) and two more amino acids (Ile135 and Glu138) from p51 subunits. Similarly, NNRTIs, including nevirapine, rilpivirine and efavirenz, showed binding interactions with the allosteric site of the enzyme and acted as non-competitive inhibitors.[22,23] These analyses hypothesized that compounds **5a** and **5b** showed similar binding interactions with the amino acid residues of the allosteric sites, so both compounds might act as non-competitive inhibitors of the HIV-1 reverse transcriptase enzyme (Fig. 8).

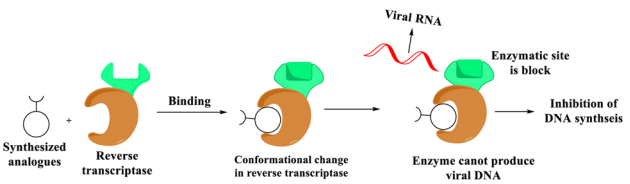


Fig. 8 Mechanism for the inhibition of reverse transcriptase *via* synthesized analogues.

### 2.7 Isothermal titration calorimetry (ITC)

ITC studies on the interaction of nevirapine and its analogues (**5a** and **5b**) with HSA protein were performed by injecting the ligand solution into the sample cell loaded with 60 μM HSA protein. The concentration of nevirapine and its analogues in the syringe was optimized (0.34 mM) to confirm the saturation of the HSA protein with the derivatives within 19 additional injections. Fig. 9 displays a representative ITC profile for the interaction of nevirapine and its analogues with HSA protein at 298 K. Fig. 9, upper panel, presents raw data as power *versus* time upon the addition of nineteen sequential injections. However, the lower panel shows the heat profile as a function of analogues to the HSA protein molar ratio.

A single set of binding site models fit the experimental results well, thereby providing the values of the stoichiometry of binding ($n$), Gibbs free energy change ($\Delta G_m$), standard molar enthalpy ($\Delta H_m$), and binding constant ($K_b$). Fig. 9 shows the obtained values of these thermodynamic parameters. The associated thermodynamic parameters of interactions of nevirapine with HSA are as $K_b = 1.0 \times 10^5\ M^{-1}$, enthalpy change $\Delta H_m = -10.6\ kJ\ mol^{-1}$, $\Delta G_m = -28.6\ kJ\ mol^{-1}$, and $n = (0.9)$. The obtained value of $K_b$ with order $10^5\ M^{-1}$ suggests the presence of strong binding between nevirapine and the HSA protein. The binding was observed to be associated with exothermic heat effects, indicating the involvement of hydrophilic interactions in the binding process since hydrophilic interactions are accompanied by exothermic heat effects. In addition, the negative $\Delta G_m$ value directly relates to the binding affinity for spontaneous binding between nevirapine and the biomolecule HSA. The nevirapine stoichiometry value (0.9) implies the binding of one molecule of nevirapine to the HSA protein. These findings of ITC investigations imply that the binding interactions of nevirapine with HSA macromolecules are thermodynamically favourable.

Next, the observed quantitative characteristics of interactions of synthesized analogues **5a** and HSA protein, including binding constant, enthalpy change, Gibbs free energy change, and stoichiometry, are $2.7 \times 10^3\ M^{-1}$, $-8.1\ kJ\ mol^{-1}$, $-19.5\ kJ\ mol^{-1}$, and 1.3, respectively.

The results suggested that the binding constant value was observed to be of the order of $10^3\ M^{-1}$, indicating that the drug molecule with $CH_3$ substitution from γ to β position binds to HSA with lesser affinity. The change in exothermic enthalpy

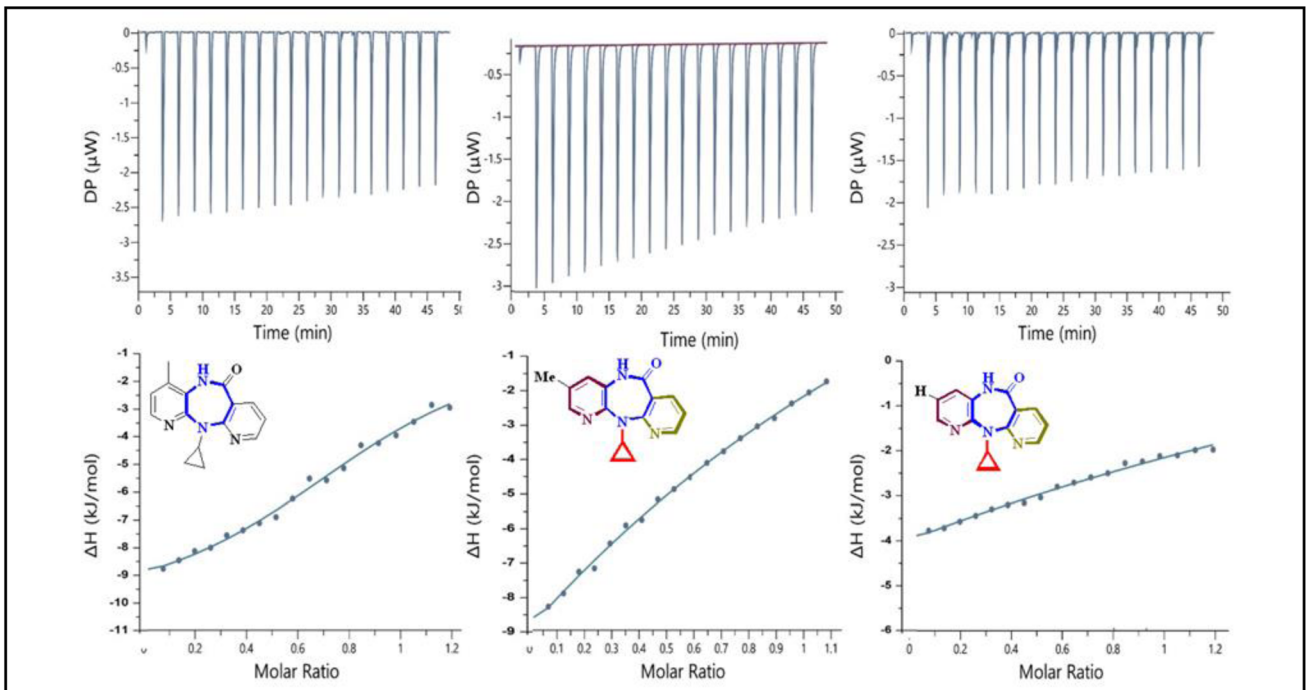


| Drug | Binding constant ($K_b$) | Enthalpy (ΔHm) KJ mol$^{-1}$ | Gibbs free energy (ΔGm) kJ mol$^{-1}$ | Stoichiometry (n) |
|---|---|---|---|---|
| **Nevirapine** | $(1.0\pm0.1) \times 10^5\ M^{-1}$ | (-10.6±0.5) | (-28.6±0.03) | (0.9±0.1) |
| **5a** | $(2.7\pm0.1) \times 10^3\ M^{-1}$ | (-8.1±0.3) | (-19.5±0.1) | (1.3±0.2) |
| **5b** | $(1.1\pm0.1) \times 10^2\ M^{-1}$ | (-4.2±0.2) | (-11.8±0.3) | (2.7±0.3) |

Fig. 9 ITC profiles for nevirapine and its analogues (**5a** and **5b**) with HSA at 298 K.

value indicates that the association process is largely driven by electrostatic interactions and the negative $\Delta G_m$ value directly relates to binding affinity for spontaneous binding. The stoichiometry value implies the binding of one molecule of compound **5a** to the HSA protein. Furthermore, the thermodynamic characteristics of interactions of compound **5b** with HSA protein in terms of a binding constant, enthalpy change, Gibbs free energy change, and stoichiometry are $1.1 \times 10^2$ $M^{-1}$, $-4.2$ kJ $mol^{-1}$, $-11.6$ kJ $mol^{-1}$, and 2.7, respectively. The effect of the substitution of $CH_3$ for H was observed on the binding constant values of the interaction with the HSA protein. The binding was observed to be least for compound **5b**, and with an exothermic enthalpy change, the binding was again observed to be spontaneous. All the analogues exhibited $\Delta H < 0$, which in turn revealed a favourable entropy contribution $\Delta S > 0$, as estimated in the calorimetric experiments. The positive and negative entropy signs confirm the ionic and electrostatic interactions between the target compound and HSA. According to the ITC results, nevirapine analogues **5b** bind weakly to HSA. This finding demonstrates that HSA is a carrier for synthesized nevirapine analogues, which are easily released in the body. This study gives accurate and thorough information about synthesized analogues binding to HSA, which can be used as a reference in anti-HIV drug binding behaviour. These findings are in agreement with the results of the study reported by Pîrnău *et al.*, 2018.[12]

### 2.8 Fluorescence quenching studies

Fluorescence quenching studies were performed to understand the binding of dipyridodiazepinone derivatives with HSA and to complement the ITC results. Fluorescence quenching studies were also performed with nevirapine to compare the effect of the methyl group position change on the binding interaction with HSA. For this, HSA was taken in a cuvette, and aliquots of nevirapine and its analogues were added to this solution. The concentrations of nevirapine and its derivative solution were increased from 0 to 0.17 mM to achieve quenching of HSA fluorescence.

To evaluate the exact quenching mechanism, the Stern–Volmer equation was applied to determine the binding constant values. The findings of the modified Stern–Volmer equation are provided in eqn (1):

$$\ln[(F_0 - F)/F] = \ln K_b + n \ln[Q] \quad (1)$$

where $F_0$ and $F$ are the fluorescence intensity of HSA in the absence and presence of the quencher, and $K_b$ is the binding constant. The quenching spectra are shown in the upper panel of Fig. 10, and Stern–Volmer plots are shown in the lower panel. Quenching spectra show the strong quenching of HSA fluorescence in the presence of nevirapine. Compound **5a** shows comparatively less quenching than nevirapine, while compound **5b** shows the least quenching of HSA fluorescence. Binding constant values obtained by plotting $\ln[(F_0 - F)/F]$ as a function of $\ln[Q]$ were $5.7 \times 10^5$ $M^{-1}$, $2.5 \times 10^3$ $M^{-1}$, and $1.1 \times 10^2$ $M^{-1}$ for nevirapine, compound **5a**, and compound **5b**, respectively. Fluorescence intensities $F$ and $F_0$ of HSA were observed at 338 nm (emission) and 280 nm (excitation), respectively. No significant shift was observed in wavelength with maximum absorbance after the addition of the quencher. Binding constant values suggest the maximum binding of nevirapine with HSA. However, changing the position of the $CH_3$ group from γ to β position in compound **5a** decreased the binding constant value with HSA. Compound **5b**, where the $CH_3$ group is being replaced by H, showed the least binding with HSA and complemented the ITC results. Fluorescence quenching analysis also confirmed that **5b** possessed poor binding affinity with HSA and was released easily in the body, which significantly influenced the ADMET mechanism.

**2.8.1 Evaluation of binding forces using thermodynamic parameters.** Thermodynamic parameters were analyzed to

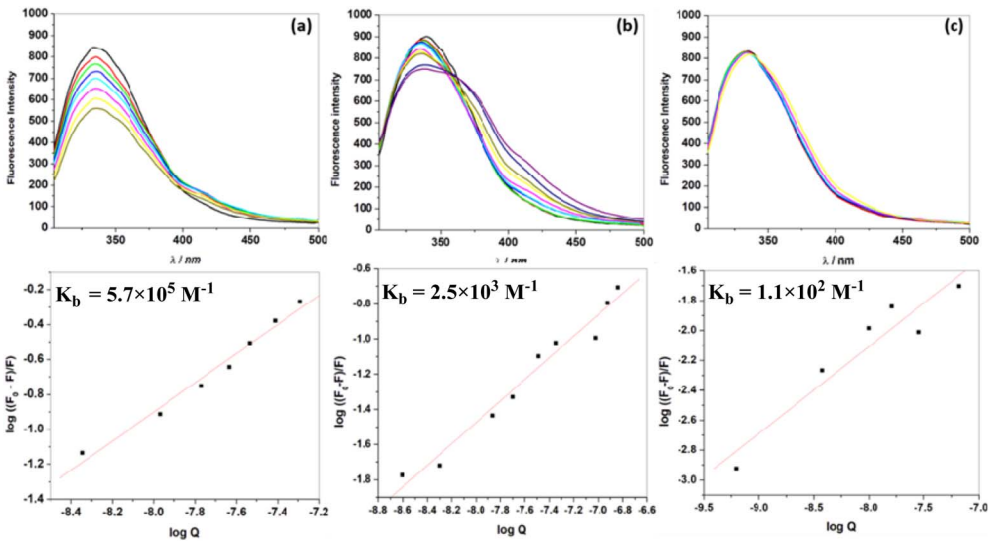


Fig. 10 Fluorescence quenching titration spectra of HSA with increasing concentrations of nevirapine (a), compound **5a** (b), and compound **5b** (c). Lower panel shows the Stern–Volmer plots of the respective compounds.

determine the type of forces involved in the macromolecule–ligand interaction. The thermodynamic parameters, including free energy change ($\Delta G$), enthalpy change ($\Delta H$), and entropy change ($\Delta S$), are crucial in determining the acting force between synthesized compounds and macromolecules, mainly including hydrophobic forces, hydrogen bonds, van der Waals forces, and electrostatic interactions. The ITC and fluorescence readings were exploited to calculate the binding affinity, $K_b$ and the number of binding sites for the synthesized compound-HSA complex. The following van't-Hoff and thermodynamic equations (eqn (2) and (3), respectively) were used to analyse the thermodynamic parameters in the binding phenomenon between the synthesized compound and HSA:

$$\log K = -\frac{\Delta H^\circ}{2.303RT} + \frac{\Delta S^\circ}{2.303R} \quad (2)$$

$$\Delta G^\circ = \Delta H^\circ - T\Delta S^\circ \quad (3)$$

Here, $T$ is the experimental temperature, $R$ is the molar gas constant and $K$ is the binding constant. The nature of the acting forces in the interaction process is as follows: (i) electrostatic/ionic interactions: $\Delta H < 0$ and $\Delta S > 0$; (ii) hydrophobic force: $\Delta H > 0$ and $\Delta S > 0$; and (iii) hydrogen and van der Waal's force: $\Delta H < 0$ and $\Delta S < 0$. It is evident from the ITC results that the calculated $\Delta G$ value is negative, which signifies that the binding of the synthesized compound with HSA is spontaneous. The entropies of the nevirapine, **5a** and **5b** were found to be +60.4, +38.26 and +25.5 J $K^{-1}$ $mol^{-1}$, respectively. The negative $\Delta H$ and positive $\Delta S$ support the electrostatic/ionic interactions with HSA and are responsible for the intrinsic fluorescence property.

# 3 Experimental section

## 3.1 Materials and instruments

All solvents, reagents, and HSA were commercially purchased from Sigma-Aldrich and used without purification. The structures of all the synthesized analogues were confirmed by applying the NMR technique. $^{13}$C NMR and $^{1}$H spectra were obtained using a Bruker spectrometer (400 MHz) with tetramethylsilane as an internal reference. A mass spectrum was recorded using a PE-SCIEX API-300 with a Turboion spray mass spectrometer. Elemental analysis was carried out using the EURO EA3000 elemental analyser instrument. The open capillary tube method was used to determine the melting points on the Buchi melting point apparatus.

## 3.2 Feature mapping analysis using a structure-based pharmacophore

The precise location of catalytic interactions between a protein and its co-crystallized ligand can be determined using a structure-based pharmacophore model. By analysing the data from this model, it is possible to identify the key pharmacophoric features that inhibit protein activity. In this case, a structure-based pharmacophore was developed based on the 3D structure of HIV-1 reverse transcriptase (PDB id: 1tkx) and its co-crystallized modulator, NAD. Using Discovery Studio 2.0, six essential pharmacophoric features were generated: hydrogen bond acceptors (HBAs), hydrophobic regions (HY), hydrogen bond donors (HBDs), and aromatic rings.[24]

## 3.3 Synthesis of nevirapine analogues

**3.3.1 Preparation of 3(a–b).** A mixture of 3-amino-2-chloro pyridine derivatives (2.4 g, 0.0187 mmol) and sodium hydrogen orthophosphate (6.25 g, 0.02 mmol) in THF-$H_2O$ was stirred at room temperature for 30 min. To this, 2-chloronicotinyol chloride (3.29 g, 0.0187 mmol) was added with continued stirring for 8 h at 60 °C to obtain a pinkish colour. Further, the reaction mixture was cooled to room temperature, extracted with ethyl acetate, and dried over anhydrous sodium sulphate, and the solvent was removed by rotatory evaporation to give crude carboxamide. It was further purified by column chromatography (silica gel 60–120 mesh size; 15–18% ethyl acetate in hexane) to give pure carboxamide.

**3a**: yield 91%, mp: 258.2–258.4 °C, IR (ATR, $\nu$/$cm^{-1}$): 3440.7 (NH), 3061.09 (C–H Ar), 2917.06 (Me), 1650.92 (CO), 1560.15 (C=N). $^{1}$H NMR (400 MHz, $CDCl_3$): $\delta$ 8.88 (s, 1H), 8.75 (s, 1H), 8.59 (d, 1H, $J$ = 6.9 Hz), 8.30 (d, 1H, $J$ = 7.64 Hz), 8.04 (s, 1H), 7.49 (t, 1H, $J$ = 7.64 Hz), 2.41 (s, 3H). $^{13}$C NMR (100 MHz, $CDCl_3$): $\delta$ 162.85, 151.96, 147.06, 144.90, 140.55, 137.72, 133.76, 130.87, 130.32, 130.02, 123.13, 18.08. MS-ESI $m/z$ (calcd/found): 281.0012/281.0123. Elemental analysis for $C_{12}H_9C_{12}N_3O$ (Calcd/Found): C(51.09/51.05), H(3.22/3.20), N(14.89/14.85).

**3b**: yield 90%, mp: 267.5–268.6 °C, IR (ATR, $\nu$/$cm^{-1}$): 3438.5 (NH), 3061 (C–H Ar), 1652.28 (CO), 1496 (C=N). $^{1}$H NMR (400 MHz, $CDCl_3$): $\delta$ 8.99 (s, 1H), 8.90 (d, 1H, $J$ = 7.96 Hz), 8.57 (d, 1H, $J$ = 4.36 Hz), 8.30 (d, 1H, $J$ = 7.52 Hz), 8.21 (d, 1H, $J$ = 4.48 Hz), 7.48 (t, 1H, $J$ = 2.1 Hz), 7.37 (t, 1H, $J$ = 2.4 Hz). $^{13}$C NMR (100 MHz, $CDCl_3$): $\delta$ 162.85, 151.96, 147.06, 144.90, 140.55, 137.72, 133.76, 130.87, 130.32, 130.02, 123.13. MS-ESI $m/z$ (calcd/found): 266.9937/266.9966. Elemental analysis for $C_{11}H_7C_{12}N_3O$ (calcd/found): C(49.28/49.25), H(2.63/2.60), N(15.67/15.60).

**3.3.2 Preparation of 5(a–h).** Sodium hydride (0.565 mmol) was washed with dry hexane. Then, substituted amine (0.3 mmol) and 10 ml dry THF were added to it at room temperature in a two-neck round-bottom flask. The reaction was stirred for 30 min, and appropriate carboxamide (1.7 mmol) was added. The reaction mixture was allowed to stir for 12 h at 60 °C. After the completion of the reaction, the reaction mixture was further cooled to room temperature and acidified with diluted HCl and extracted with ethyl acetate (2 × 10 ml). All organic layers were combined, dried over anhydrous sodium sulphate, and concentrated under vacuum to produce crude dipyridodiazepinone. The crude compound was purified from column chromatography (silica gel 60–120 mesh size, 10–14% ethyl acetate in hexane) to give pure dipyridodiazepine **5(a–h)**.

**5a**: yield 88%, mp: 244.4–244.8 °C, IR (ATR, $\nu$/$cm^{-1}$): 3440.7 (NH), 3061.09(C–H, Ar), 2917.06 ($CH_3$), 1650.92 (CO). $^{1}$H NMR (400 MHz, $CDCl_3$): $\delta$ 8.62 (s, 1H), 8.29 (d, 1H, $J$ = 4.2 Hz), 8.12 (d, 1H, $J$ = 7.12 Hz), 7.72 (s, 1H), 7.37 (s, 1H), 6.92 (t, 1H, $J$ = 6 Hz), 2.44 (s, 3H), 2.25 (m, 1H), 0.84 (m, 2H), 0.69 (m, 2H). $^{13}$C NMR (100 MHz, $CDCl_3$): $\delta$ 162.82, 151.99, 147.03, 144.69, 140.53,

138.68, 130.20, 129.43, 123.38, 123.11, 122.39, 23.86, 18.96 7.24, 7.16. MS-ESI *m*/*z* (calcd/found): 266.3040/266.1168. Elemental analysis for $C_{15}H_{14}N_4O$ (calcd/found): C(67.65/67.60), H(5.30/5.25), N(21.04/21.02).

**5b**: yield 84%, mp: 247.2–257.9 °C, IR (ATR, $\nu$/cm$^{-1}$): 3438.5 (NH), 3061.09 (CH–Ar), 1652.28 (CO). $^1$H NMR (400 MHz, $CDCl_3$): $\delta$ 8.86 (s, 1H), 8.31 (d, 1H, $J$ = 3.6 Hz), 8.05 (dd, 2H, $J$ = 2.48 Hz), 7.59 (d, 1H, $J$ = 2.48 Hz), 7.19 (t, 1H, $J$ = 5.8 Hz), 6.94 (t, 1H, $J$ = 8 Hz), 2.22 (m, 1H), 0.79 (m, 2H), 0.58 (m, 2H). $^{13}$C NMR (101 MHz, $CDCl_3$): $\delta$ 162.82, 151.99, 147.03, 144.69, 140.65, 138.68, 130.20, 129.43, 123.38, 123.11, 122.39, 23.86, 7.24, 7.16. MS-ESI *m*/*z* (calcd/found): 252.2770/252.1011. Elemental analysis for $C_{14}H_{12}N_4O$ (calcd/found): C(66.65/62.55), H(4.79/4.75), N(22.21/22.20).

**5c**: yield 83%, mp: 243.5–243.8 °C, IR (ATR, $\nu$/cm$^{-1}$): 3440.7 (NH), 3061.09 (CH Ar), 2917.06 (Me), 1650.92 (CO). $^1$H NMR (400 MHz, $CDCl_3$): $\delta$ 8.91 (s, 1H), 8.31 (d, 1H, $J$ = 3.6 Hz), 8.25 (d, 1H, $J$ = 6.2 Hz), 7.99 (s, 1H), 7.58 (s, 1H), 6.95 (t, 1H, $J$ = 4.5 Hz), 3.47 (m, 1H), 2.35 (m, 2H), 2.30 (s, 3H), 2.07 (m, 4H). $^{13}$C NMR (100 MHz, $CDCl_3$): 169.26, 166.75, 147.83, 147.27, 141.74, 139.06, 136.82, 127.65, 125.14, 120.22, 114.49, 56.34, 30.08, 18.76. MS-ESI *m*/*z* (calcd/found): 280.1324/280.1321. Elemental analysis for $C_{16}H_{16}N_4O$ (calcd/found): C (68.55/68.50), H (5.75/5.71), N(19.99/19.95).

**5d**: yield: 82%, mp: 225.1–225.2 °C, IR (ATR, $\nu$/cm$^{-1}$): 3438.5 (NH), 3061.09 (C–H Ar), 1652.28 (CO), 1496.44 (C=N). $^1$H NMR (400 MHz, $CDCl_3$): $\delta$ 9.11 (s, 1H), 8.47 (d, 1H, $J$ = 3.64 Hz), 8.18 (d, 1H, $J$ = 3.52 Hz), 8.01 (d, 1H, $J$ = 3.52 Hz), 7.62 (d, 1H, $J$ = 2.4 Hz), 6.99 (t, 1H, $J$ = 6.04 Hz), 6.88 (t, 1H, $J$ = 5.96 Hz), 3.47 (m, 1H), 2.36 (m, 2H), 2.12 (m, 2H), 1.94 (m, 2H). $^{13}$C NMR (100 MHz, $CDCl_3$): 169.26, 166.75, 147.83, 147.27, 141.74, 139.06, 136.77, 127.65, 125.14, 120.22, 114.49, 50.15, 18.76, 13.77. MS-ESI *m*/*z* (calcd/found): 266.1168/266.1165. Elemental analysis for $C_{15}H_{14}N_4O$ (calcd/found): C(67.65/67.65), H(5.30/5.25), N(21.04/21.01).

**5e**: yield 80%, mp: 225.1–225.2 °C, IR (ATR, $\nu$/cm$^{-1}$): 3397 (NH), 2926.1 (CH Ar), 1650.5 (CO), 1496.44 (C=N). $^1$H NMR (400 MHz, $CDCl_3$): $\delta$ 8.31 (s, 1H), 8.15 (d, 1H, $J$ = 5.4 Hz), 7.89 (d, 1H, $J$ = 6.2 Hz), 7.66 (s, 1H), 7.47 (s, 1H), 6.75 (t, 1H, $J$ = 4.9 Hz), 3.02 (m, 1H), 2.23 (s, 3H), 1.86 (m, 2H), 1.56 (m, 6H). $^{13}$C NMR (100 MHz, $CDCl_3$): 169.26, 166.75, 147.83, 147.27, 141.74, 139.06, 136.77, 127.65, 125.14, 120.22, 114.49, 61.82, 34.70, 25.66, 18.76. MS-ESI *m*/*z* (calcd/found): 294.1481/294.1475. Elemental analysis for $C_{17}H_{18}N_4O$ (calcd/found): C(69.37/69.35), H(6.16/6.14), N(19.03/19.01).

**5f**: yield 81%, mp: 222.1–222.4 °C, IR (ATR, $\nu$/cm$^{-1}$): 3438.5 (NH), 3061.9 (C–H Ar), 1652.28 (CO), 1496.44 (C=N). $^1$H NMR (400 MHz, $CDCl_3$): $\delta$ 8.80 (s, 1H), 8.22 (d, 1H, $J$ = 2.36 Hz), 7.98 (d, 1H, $J$ = 6.9 Hz), 7.90 (d, 1H, $J$ = 2.36 Hz), 7.52 (d, 1H, $J$ = 3.56 Hz), 6.90 (t, 1H, $J$ = 5.88 Hz), 6.77 (t, 1H, $J$ = 6.16 Hz), 3.02 (m, 1H), 1.85 (m, 2H), 1.58 (m, 6H). $^{13}$C NMR (100 MHz, $CDCl_3$): 169.26, 166.75, 149.04, 147.83, 142.78, 139.06, 134.91, 129.21, 120.22, 120.13, 114.49, 61.82, 34.70, 25.66. MS-ESI *m*/*z* (calcd/found): 280.1324/280.1322. Elemental analysis for $C_{16}H_{16}N_4O$ (calcd/found): C(68.55/68.51), H(5.75/5.73), N(19.99/19.95).

**5g**: yield 83%, mp: 220.4–220.5 °C, IR (ATR, $\nu$/cm$^{-1}$): 3324.06 (NH), 3142.34 (CH–Ar), 2920.77(Me), 2851.32 (alkyl), 1666.73 (CO). $^1$H NMR (400 MHz, $CDCl_3$): $\delta$ 8.50 (s, 1H), 8.14 (d, 1H, $J$ = 3.6 Hz), 8.04 (d, 1H, $J$ = 3.56 Hz), 7.59 (s, 1H), 7.30 (s, 1H), 6.86 (t, 1H, $J$ = 5.92 Hz), 4.25 (dt, 2H, $J$ = 4.2 Hz), 2.29 (s, 3H), 1.61 (m, 2H), 1.04 (t, 3H, $J$ = 5.32 Hz). $^{13}$C NMR (100 MHz, $CDCl_3$): 169.26, 167.48, 148.38, 146.64, 142.76, 139.24, 135.76, 127.96, 127.48, 121.76, 113.95, 46.25, 21.13, 18.76, 11.99. MS-ESI *m*/*z* (calcd/found): 268.1324/268.1321. Elemental analysis for $C_{15}H_{16}N_4O$ (calcd/found): C(67.15/67.12), H(6.01/6.04), N(20.88/20.80).

**5h**: yield 82%, mp: 221.2–221.4 °C, IR (ATR, $\nu$/cm$^{-1}$): 3314.95 (NH), 3060.03 (CH–Ar), 2924.85 (Me), 1670.12 (CO), 1495.13 (C=N). $^1$H NMR (400 MHz, $CDCl_3$): $\delta$ 8.84 (s, 1H), 8.17 (d, 1H, $J$ = 5.8 Hz), 8.16 (dd, 2H, $J$ = 7.5 Hz), 7.91 (d, 1H, $J$ = 6.4 Hz), 6.87 (t, 1H, $J$ = 4.5 Hz), 6.74 (t, 1H, $J$ = 5.4 Hz), 4.04 (dt, 2H, $J$ = 4.6 Hz), 1.75 (m, 2H), 1.06 (t, 3H, $J$ = 5.32 Hz). $^{13}$C NMR (100 MHz, $CDCl_3$): 169.26, 167.48, 148.38, 148.08, 144.04, 139.24, 133.86, 129.73, 122.09, 121.76, 113.95, 46.25, 21.13, 11.99. MS-ESI *m*/*z* (calcd/found): 254.1168/254.1164. Elemental analysis for $C_{14}H_{14}N_4O$ (calcd/found): C(66.13/66.12), H(5.55/5.51), N(22.03/22.01).

### 3.4 HIV-1 reverse transcriptase inhibitory study

The effect of synthesized analogues was determined using the RT assay colorimetric kit (MyBioSource, Cat MBS412605) as per the instructions of the manufacturer. Briefly, reaction buffer and HIV RT reverse transcriptase enzyme solution were added to microfuge tubes containing different concentrations (1, 10, 50, and 100 nM) of nevirapine and its analogues. Lysis buffer, reaction buffer, and HIV reverse transcriptase were used without treatment as negative controls. After 20 min incubation at 37 °C, 100 μl of each reaction mixture was transferred to a streptavidin-coated microwell and again incubated for 20 min at 37 °C. Before adding 100 μl of HRP Anti Digoxigenin Conjugate, the ELISA plate was completely washed 5 times with wash buffer. A further 45 min incubation was followed by washing again 5 times using wash buffer at 37 °C. 100 μl of ABTS substrate solution was added to the wells and incubated for 30 min at 37 °C until the development of colour was sufficient to detect using an ELISA plate reader at 405 nm. Otherwise, the addition of 25 μl of stop solution can also be used to terminate the reaction and then read the absorbance at 405 nm.[25]

### 3.5 Molecular docking

The computational technique of molecular docking is utilized to examine the interaction between ligands and macromolecules. The three-dimensional (3D) structure of HIV-1 reverse transcriptase (PDB id: 1tkx) was retrieved from the **https://www.rcsb.org/protein** data bank site. Further, the macromolecule's 3D structure was opened in Discovery Studio Visualizer, hydrogen atoms were added, water molecules were removed, and valency was satisfied and saved in the PDBQT format.[26,27] Subsequently, both ligands (**5a**, **5b**, and nevirapine) and macromolecules were subjected to a PyRx window to predict the binding interaction using the AutoDock Vina module.[28] Other parameters remained at their default values, except the grid box modified following the active sites of individual macromolecules. Additionally, the ligand's bonds were permitted to rotate unrestrictedly, resulting in

a rigid receptor. After the molecular docking study was completed and 10 configurations for each drug–protein complex were constructed for all synthesized analogues, text files with scoring results were generated for manual comparison. The docking poses with weaker binding energy were believed to be the best. Using Discovery Studio Visualizer and PyMol, the interaction between ligands and macromolecules was analyzed and visualized.

### 3.6 Drug-like, physicochemical, and ADMET properties

Lipinski's rule of five criteria was used to evaluate the potential drug-likeness of each ligand. The ADMETSar web tool was used to validate Lipinski's rule of five parameters. To evaluate the pharmacodynamics of a potential drug candidate, it is necessary to consider the ADMET mechanism of the molecule.[29] After molecular docking, ADMETSar and SWISSADME servers were used to predict the ADMET mechanism of the nevirapine analogues. The SMILES format of the ligand structure was used in the web server.

### 3.7 Molecular dynamics simulations

MD simulations were conducted with the GROMACS 2020 software to evaluate the credibility of the docking results.[30,31] The simulations used the CHARMM36 force field, TIP3P water model, and CHARMM36-Feb 2021 update version.[13] Proteins, namely, 5dyw and 4ey7, were placed together with their respective complexes and positioned in the geometric center of a dodecahedron-shaped container. The distance between the protein complexes and the edges of the container was set at 10 Å. To achieve system neutralization at this step, negative ions ($Cl^-$) and positive ions ($Na^+$) were introduced parallelly by displacing the solvent molecules as required. Then energy minimization procedure was conducted using the Verlet cutoff methodology to mitigate steric hindrances inside the system. Further, the energy minimum was conducted using the steepest descent method with a maximum step size of 50 000 to ensure the absence of atomic collisions. Furthermore, equilibrium states were achieved by 100 ns NPT and NVT simulations at a pressure of 1 ATM and at a temperature of 300 kelvin. Subsequently, a molecular simulation lasting 10 ns was conducted. Following MD simulation, an investigation of several properties, such as Radius of Gyration (Rg), Root Mean Square Deviation (RMSD), and Root Mean Square Fluctuation (RMSF), was performed on the trajectory. These properties were obtained using the built-in capabilities provided by Desmond software.

### 3.8 Isothermal titration calorimetry (ITC)

To analyse the energetics of the interaction of nevirapine within the solution, ITC is recognized as the gold standard experimental device. ITC offers accurate, quick, and easy label-free monitoring of the thermodynamics of molecular interactions by determining the heat gained or released during interactions.[32] Therefore, MICRO CAL PEAQ-ITC (Malvern) is used to determine the thermodynamics of the interactions of ligands with the macromolecule.[33,34] The calibration of ITC was performed before running the experiments with standard EDTA and $Ca^{2+}$ solutions, and binding parameters matched well with the standard thermodynamic parameters of Ca–EDTA binding. The exact concentration of macromolecule (HSA) and synthesized compounds required for ITC experiments was determined using a UV-Visible spectrophotometer from SHIMADZU at 280 nm ($A_{1cm}{}^{1\%} = 5.3$). All the solutions were prepared in 5% DMSO solution in 20 mM phosphate buffer (pH = 7.4) for microcalorimetric experimental analysis. The same solution was also used in the reference cell to evaluate the thermodynamic properties associated with the interactions. The macromolecule solution in the sample cell was titrated with the ligand solution filled in a computer-controlled syringe. A syringe (40 μl) was used to inject the ligand solution into the sample cell that contained 200 μl of macromolecules. Dilution experiments were conducted by titrating the syringe solution (**5a**, **5b** and nevirapine) against a similar buffer. The final heat reported in the ITC profiles was calculated by subtracting the heat produced in the dilution experiment from the primary titration profile. At the end of titration, the concentration in the syringe was adjusted to achieve saturated heat for each experiment. The experiment was programmed for 19 consecutive injections, with the first injection 0.4 μl, followed by 18 subsequent injections (2 μl), at 150-second time intervals. For all titrations throughout the run, a stirring speed of 750 rpm was fixed for the syringe.

**3.8.1 Calculation.** To analyse the data, the Micro CAL PEAQ ITC analysis software provided with the instrument was used. The association constant ($K_a$) and binding stoichiometry ($n$), as well as the entropy and enthalpy changes ($\Delta S$ and $\Delta H$), during drug macromolecule interaction were obtained directly from the ITC instrument. The changes in the free energy value $\Delta G$ were subsequently calculated using the following equation:

$$\Delta G = \Delta H - T\Delta S \quad (4)$$

### 3.9 Fluorescence spectroscopy

A PerkinElmer model LS45 spectrofluorometer was used to measure the intrinsic fluorescence of HSA in the presence of nevirapine analogs in a quartz cell of 3 ml capacity and path length of 1 cm. The protein concentration in all experiments was kept constant. The excitation and emission slits were fixed at 10 nm. The wavelength of excitation was fixed at 280 nm, and the emission spectra were recorded in the wavelength range of 300–500 nm at a scan rate of 600 nm $min^{-1}$. For this, HSA and drug solutions were made in 5% DMSO solution in 20 mM phosphate buffer to achieve the required solubility of nevirapine and its analogous for quenching studies.[35]

## 4 Conclusion

In the present study, novel dipyridodiazepinone (nevirapine) analogue **5(a–h)** was synthesized using a simple and efficient base-promoted C–N coupling reaction assisted by amination amidation and cyclocondensation reactions. Synthesized analogues were analyzed by employing feature mapping analysis using structure-based pharmacophore design, molecular

docking and *in vitro* HIV-1 reverse transcriptase inhibitory activity, MD simulation and *in silico* pharmacokinetic properties utilizing the ADMETSar web tool. Further, thermodynamic and spectroscopic analyses of the synthesized analogues were conducted using an ITC experiment to understand their binding interactions with HSA.

The feature mapping analysis and molecular docking studies indicated that compounds **5a** and **5b** possess good fit value and affinity towards HIV-1 reverse transcriptase and showed considerable interaction with key residues such as hydrogen residue (Lys101), pi–sigma residue (Leu100), alkyl and pi–alkyl residues (Lys103, Tyr181, Val106, Leu234, and Tyr188) available at the catalytic site of enzyme. Furthermore, based on ADMET and physicochemical analysis, the results indicate that compound **5b** had favourable pharmacokinetic characteristics and drug-like properties. Most notably, both compounds exhibited considerable safety in toxicity assessments. The findings from ITC revealed key interactions between the synthesized analogues and HSA protein, which in turn indicated the possibility of their expedited transportation and associated therapeutic effect in the recipient. In conclusion, these findings suggest that these compounds have significant HIV-1 reverse transcriptase inhibitory activities and possess drug-like properties and thus need immediate in-depth exploration for their utility as therapeutic agents in the management of HIV-1-mediated diseases.

## Author contributions

SJ: investigation and writing original draft; SJ: molecular docking studies; AM: fluorescence and ITC studies; KV: *in vitro* studies; SoJ: data validation; DK: project administration; JD: supervision, conceptualization and manuscript editing; SS: supervision and manuscript editing.

## Conflicts of interest

The authors declare that they have no known competing financial interests or personal relationships that could have appeared to influence the work reported in this paper.

## Data availability

The data supporting this article have been included as part of the SI. IR, HSQC, $^{1}$H NMR, $^{13}$C NMR, mass. See DOI: **https://doi.org/10.1039/d5ra03504j**.

## Acknowledgements

The authors acknowledge the Department of Science and Technology (DST-FIST, India, Order Number SR/FST/2022/252) for providing all the necessary facilities. The author would also like to thank Prof. Ina Aditya Shastri, Vice-Chancellor of Banasthali Vidyapith, Rajasthan, India, for the successful accomplishment of the present work.

## References

1 A. Leśniewska and P. Przybylski, *Eur. J. Med. Chem.*, 2024, **275**, 116556.
2 Y. Malki, J. Martinez and N. Masurier, *Med. Res. Rev.*, 2021, **41**, 2247–2315.
3 S. Jaiswal, D. Kishore, A. Bhardwaj, K. Bhardwaj, S. Richa, S. Jain, J. Dwivedi and S. Sharma, *Org. Biomol. Chem.*, 2024, **22**, 6520–6531.
4 L. D. Fader, S. Landry, S. Morin, S. H. Kawai, Y. Bousquet, O. Hucke, N. Goudreau, C. T. Lemke, P. Bonneau, S. Titolo and S. Mason, *Bioorg. Med. Chem. Lett.*, 2013, **23**, 3396–3400.
5 D. Bellarosa, G. Antonelli, F. Bambacioni, D. Giannotti, G. Viti, R. Nannicini, A. Giachetti, F. Dianzani, M. Witvrouw, R. Pauwels and J. Desmyter, *Antiviral Res.*, 1996, **30**, 109–124.
6 L. D. Fader, R. Bethell, P. Bonneau, M. Bös, Y. Bousquet, M. G. Cordingley, R. Coulombe, P. Deroy, A. M. Faucher, A. Gagnon and N. Goudreau, *Bioorg. Med. Chem. Lett.*, 2011, **21**, 398–404.
7 W. Guo, M. Zhao, W. Tan, L. Zheng, K. Tao and X. Fan, *Org. Chem. Front.*, 2019, **6**, 2120–2141.
8 K. Bhardwaj, S. Jaiswal, A. Bhardwaj, D. Arora, S. Jain, G. Kumar, J. Dwivedi and S. Sharma, *J. Mol. Struct.*, 2025, **1336**, 142105.
9 N. Yaduvanshi, S. Tewari, S. Jaiswal, M. Devi, S. Shukla, J. Dwivedi and S. Sharma, *Inorg. Chem. Commun.*, 2024, **161**, 111927.
10 A. Bhardwaj, S. Jaiswal, K. Verma, K. Bhardwaj, M. Sharma, S. Jain, J. Dwivedi and S. Sharma, *Chem. Rec.*, 2025, **25**, 202400156.
11 G. Bec, B. Meyer, M. A. Gerard, J. Steger, K. Fauster, P. Wolff, D. Burnouf, R. Micura, P. Dumas and E. Ennifar, *J. Am. Chem. Soc.*, 2013, **135**, 9743–9752.
12 A. Pîrnău, M. Mic, S. Neamţu, C. G. Floare and M. Bogdan, *Spectrochim. Acta, Part A*, 2018, **191**, 226–232.
13 S. Jaiswal, M. Devi, N. Yaduvanshi, S. Jain, J. Dwivedi, D. Kishore, A. E. Kuznetsov and S. Sharma, *J. Mol. Struct.*, 2024, **1314**, 138734.
14 L. Guan, H. Yang, Y. Cai, L. Sun, P. Di, W. Li, G. Liu and Y. Tang, *Medchemcomm*, 2019, **10**, 148–157.
15 A. Kaur, K. Kaur, P. K. Banipal and T. S. Banipal, *J. Chem. Thermodyn.*, 2021, **152**, 106269.
16 N. E. Alshaikh, M. Zaki, A. A. Sharfalddin, N. S. Al-Radadi, M. A. Hussien and W. M. Hassan, *Arabian J. Chem.*, 2023, **16**, 104845.
17 W. L. Jorgensen, M. Bollini, V. V. Thakur, R. A. Domaoal, K. A. Spasov and K. S. Anderson, *J. Am. Chem. Soc.*, 2011, **133**, 15686–15696.
18 M. H. R. Molla, A. H. Asseri and M. S. Islam, *Egypt. J. Med. Hum. Genet.*, 2023, **24**, 51.
19 M. Mahboubi-Rabbani, M. Abbasi, Z. Hajimahdi and A. Zarghi, *Iran. J. Pharm. Res.*, 2021, **20**, 333–369.
20 J. M. Seckler, M. D. Barkley and P. L. Wintrode, *Biophys. J.*, 2011, **100**, 144.

21 P. Chandra, S. Ganguly and S. Karmakar, *Chem. Proc.*, 2021, **3**, 33.
22 M. J. Kim, K. L. Yu, R. Han, Y. Lee, K. Oh and J. C. You, *ACS Infect. Dis.*, 2023, **9**, 1582–1592.
23 A. K. Singh, A. Kumar, S. Arora, R. Kumar, A. Verma, H. Khalilullah, M. Jaremko, A. H. Emwas and P. Kumar, *Chem. Biol. Drug Des.*, 2024, **103**, e14372.
24 S. Jain, S. Sharma, A. Paliwal, J. Dwivedi, S. Paliwal, V. Paliwal, S. Paliwal and J. Sharma, *Med. Chem. Res.*, 2023, **33**, 1–15.
25 M. Devi, S. Jaiswal, N. Yaduvanshi, N. Kaur, D. Kishore, J. Dwivedi and S. Sharma, *ChemistrySelect*, 2023, **8**, 202204710.
26 S. Sain, S. Jaiswal, S. Jain, N. Misra, A. Srivastava, R. Jendra, D. Kishore, J. Dwivedi, S. M. Wabaidur, M. A. Islam and S. Sharma, *Chem. Biodivers.*, 2022, **19**, 202200540.
27 M. Devi, S. Jaiswal, N. Yaduvanshi, S. Jain, S. Jain, K. Verma, R. Verma, D. Kishore, J. Dwivedi and S. Sharma, *J. Mol. Struct.*, 2023, **1286**, 135571.
28 K. Verma, S. Makwana, S. Paliwal, V. Paliwal, S. Jain, S. Paliwal and S. Sharma, *Curr. Res. Pharmacol. Drug Discovery*, 2022, **3**, 100088.
29 A. M. Wensing, V. Calvez, F. Ceccherini-Silberstein, C. Charpentier, H. F. Günthard, R. Paredes, R. W. Shafer and D. D. Richman, *Antiviral Med.*, 2022, **30**, 559.
30 R. S. K. Vijayan, E. Arnold and K. Das, *Proteins: Struct., Funct., Bioinf.*, 2014, **82**, 815–829.
31 S. Jaiswal, K. Verma, J. Dwivedi and S. Sharma, *Eur. J. Med. Chem.*, 2024, **271**, 116388.
32 X. Zhou, Q. Yang, X. Xie, Q. Hu, F. Qi, Z. U. Rahman and X. Chen, *Dyes Pigm.*, 2012, **92**, 1100–1107.
33 P. K. Gharai, J. Khan, K. Pradhan, R. Mallesh, S. Garg, M. U. Arshi, S. Barman and S. Ghosh, *ACS Chem. Neurosci.*, 2024, **15**(13), 2470–2483.
34 P. K. Gharai, J. Khan, R. Mallesh, S. Garg, S. Gupta, P. Jaisankar and S. Ghosh, *ACS Chem. Neurosci.*, 2025, **16**, 2224–2236.
35 M. Kurmi, A. Sahu, A. Balhara, I. P. Singh, S. Kulkarni, N. K. Singh, P. Garg and S. Singh, *J. Pharm. Biomed. Anal.*, 2020, **178**, 112911.